2013 European Control Conference (ECC)
July 17-19, 2013, Zürich, Switzerland.

Position Trajectory Tracking of a Quadrotor Helicopter based on L1 Adaptive Control

Paul De Monte and Boris Lohmann

Abstract— **We present an adaptive backstepping controller for the position trajectory tracking of a quadrotor. The tracking controller is based on the L1 adaptive control approach and uses a typical nonlinear quadrotor model. We slightly modify the L1 adaptive control design for linear systems to comply with the time-varying nonlinear error dynamics that arise from the backstepping design. Our approach yields a stable adaptive system with verifiable bounds on the tracking error and input signals. The adaptive controller compensates for all model uncertainties and for all bounded disturbances within a particular frequency range, which we specify a priori. The design of this frequency range involves a trade-off between control performance and robustness, which can be managed transparently through the L1 adaptive control design. Simulation results show the powerful properties of the presented control application.**

I. Introduction

Trajectory tracking control for quadrotor helicopters and other vertical take-off and landing vehicles (VTOLs) has become a broad field of research during the last few decades. One reason is their high potential for aerial survey or search and rescue missions. Another reason is the challenge associated with the control design, because VTOLs are usually underactuated and highly nonlinear.

The application of nonlinear control approaches such as feedback linearization [1], sliding mode control [2] and forwarding [3] allows a wide range of flight maneuvers beyond hovering. Backstepping [4] in particular is a useful and often applied approach [5], [6] since the design procedure is very well suited to the cascaded plant structure of VTOLs.

In recent years, researchers have begun to integrate adaptation in their control designs for VTOLs in order to achieve a higher accuracy and robustness given in presence of model uncertainties and external disturbances. For example, many control designs omit aerodynamic effects, which are hard to identify, from their plant model. Thus one objective is to estimate and compensate for the aerodynamic effects [7], [8]. Other approaches consider and cancel out constant disturbances [9], [10] or compensate for unknown model parameters [11].

Standard model reference adaptive control (MRAC) [12] is a famous approach, but without additional augmentations, e.g. [13], [14], the architecture suffers from certain drawbacks. With fast adaptation, MRAC is prone to responding to high-frequency excitations, and when the adaptive estimates are directly used for control, fast adaptation leads to high gain feedback and harms the robustness margin. Thus the designer is restricted to slow adaptation, which in turn causes large transients and slow convergence [15].

L1 adaptive control [16], [17] extends the state-predictor-based MRAC and handles the trade-off between performance and robustness with fast adaptation in a transparent and effective way. L1 adaptive control does not necessarily compensate for uncertainties in the whole frequency domain. The designer can decide up to which frequency the controller should react to uncertainties. Hence the control inputs are not affected by high frequency excitations and can meet actuator limitations. Furthermore, the design guarantees verifiable bounds on the system's states and input signals. In summary, L1 adaptive control is an appealing approach for practical applications, where one has to meet a realistic trade-off between performance and robustness.

The contribution of this work: We present a backstepping approach for the position trajectory tracking problem of a quadrotor helicopter, which is extended by the L1 adaptive control architecture. Since the backstepping design inevitably results in a time-varying nonlinear system for the error dynamics, the L1 adaptive control design for linear reference models [16] is not exactly applicable. Thus we present a slight design modification, which preserves the majority of the well-understood design procedure available for linear reference models. By means of the L1 adaptive control design, our controller is able to compensate for all model parameter uncertainties and all bounded disturbances within a selected frequency range. We derive a sufficient condition for closed-loop stability and determine the upper bounds for the system's states, estimation errors and control inputs.

The remainder of the paper is organized as follows: Section II introduces the quadrotor model used for the control design. Section III presents the backstepping control design and the application of L1 adaptive control. Section IV provides simulation results.

Special notations: The superscript $'$ is used throughout this paper to indicate the transpose of a vector or matrix. For signals in the time domain, we always drop the argument t, whereas for signals in the frequency domain, we always write the argument s.

II. Quadrotor model

In this section, we present the quadrotor's dynamic equations used for the control design. Quadrotors are powered by four rotors symmetrically arranged at each end of a cross-shaped frame, see Fig. 1. The rotation speed of the four

P. De Monte and B. Lohmann are with the Institute of Automatic Control, Technische Universität München, 85748 Garching b. München, Germany paul.demonte@tum.de, lohmann@tum.de

This work is supported by the German Federal Ministry of Economics and Technology.

rotors is usually controlled by embedded motor controllers, which offer very fast dynamics. Thus many control designs as well as our design neglect these dynamics. The four rotor speeds produce one total thrust for the translational acceleration and three torque components for the rotation of the vehicle. One can either consider the four rotor speeds or equivalently the total thrust and the torque as control inputs. The relation between the input commands and the actual effective thrust and torque carries uncertain parameters, depending, for instance, on the chosen propeller type, the motor efficiencies and the quadrotor geometry. In order to compensate for these uncertainties, we consider uncertain input gains in our plant model. For the derivation of the

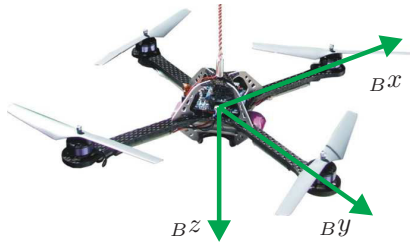

Fig. 1. Quadrotor helicopter with body-fixed coordinate frame B.

dynamic equations, the quadrotor is treated as a rigid body and the rotors' gyroscopic effect is neglected, since it is of minor importance for the dynamic behavior. We write the translational dynamics with respect to an inertial north-east-down coordinate frame as

$$\dot{\mathbf{x}} = \boldsymbol{v} \,, \tag{1}$$

$$\dot{\boldsymbol{v}} = \mathbf{f}(\boldsymbol{v}) + g\mathbf{e}_z - \kappa_v \, \mathbf{T} + \boldsymbol{\zeta}_v \,, \tag{2}$$

where $\mathbf{x} = [x \; y \; z]'$ and $\boldsymbol{v} = [\dot{x} \; \dot{y} \; \dot{z}]'$ are the position and the velocity, g is the gravity constant, $\mathbf{e}_z = [0 \; 0 \; 1]'$ the unit vector pointing in the inertial ${}_I z$-direction and $\mathbf{T} = T\,\mathbf{R}\mathbf{e}_z$ is the total thrust given in the inertial system with the thrust magnitude T and the rotation matrix $\mathbf{R} \in SO(3) := \{\mathbf{R} \in \mathbb{R}^{3\times3} | \mathbf{R}'\mathbf{R} = \mathbf{I}_{3\times3}, \det(\mathbf{R}) = 1\}$ from the body-fixed coordinate frame into the inertial coordinate frame. The function $\mathbf{f}(\boldsymbol{v})$ is Lipschitz-continuous in $\boldsymbol{v}$ and models drag forces. The parameter κ_v considers the uncertainty involved in the actuation, and $\boldsymbol{\zeta}_v$ is an unknown time-varying, piecewise-continuous and bounded disturbance.

The use of the rotation matrix as an element of the special orthogonal group $SO(3)$, yields a singularity free and globally unique attitude parametrization [5] and thus is employed in this work. The kinematics for the attitude parameters is

$$\dot{\mathbf{R}} = \mathbf{R}\underline{\boldsymbol{\omega}} \,, \tag{3}$$

where $\boldsymbol{\omega} = [\omega_x \; \omega_y \; \omega_z]'$ is the quadrotor's angular velocity and the map $\_ : \mathbb{R}^3 \to \mathbb{S}$ transforms a vector in $\mathbb{R}^3$ to the space of skew-symmetric matrices $\mathbb{S} := \{S \in \mathbb{R}^{3\times3} | S = -S'\}$ such that $\underline{\mathbf{a}}\mathbf{b} = \mathbf{a} \times \mathbf{b}$ holds. In order to control the translational movement of the quadrotor, we can use $\boldsymbol{\omega}_{xy} = [\omega_x \; \omega_y]'$ and $\dot{T}$ to influence the thrust vector $\mathbf{T}$. The corresponding relation is given by

$$\begin{aligned}\dot{\mathbf{T}} &= \dot{T}\,\mathbf{R}\mathbf{e}_z + T\mathbf{R}\underline{\boldsymbol{\omega}}\mathbf{e}_z = \dot{T}\,\mathbf{R}\mathbf{e}_z - T\mathbf{R}\underline{\mathbf{e}}_z\boldsymbol{\omega} \\ &= \underbrace{\mathbf{R}\begin{bmatrix}-T\underline{\mathbf{e}}_{z1} & -T\underline{\mathbf{e}}_{z2} & \mathbf{e}_z\end{bmatrix}}_{\mathbf{M}(\mathbf{R},T)} \begin{bmatrix}\omega_x & \omega_y & \dot{T}\end{bmatrix}' \,, \end{aligned} \tag{4}$$

where $\underline{\mathbf{e}}_{z1}$ and $\underline{\mathbf{e}}_{z2}$ are the first and second column of the skew-symmetric matrix for $\mathbf{e}_z$. Note that $\underline{\mathbf{e}}_{z3} = [0 \; 0 \; 0]'$ holds. The angular velocity ω_z has no influence on the translational dynamics and can independently be used to control the heading dynamics. Provided desired values for $\boldsymbol{\omega}$ are available, one can use Euler's equations

$$\dot{\boldsymbol{\omega}} = \mathbf{J}^{-1}(\mathbf{J}\boldsymbol{\omega} \times \boldsymbol{\omega}) + \boldsymbol{\kappa}_\omega \boldsymbol{\tau} + \boldsymbol{\zeta}_\omega \,, \tag{5}$$

to access both, $\dot{\omega}_z$ for the heading control and $\dot{\boldsymbol{\omega}}_{xy}$ for the position tracking. In (5), $\mathbf{J}$ is the moment of inertia and $\boldsymbol{\tau} = [\tau_x \; \tau_y \; \tau_z]'$ are the three torque components, which are regarded as control inputs. Through $\boldsymbol{\kappa}_\omega$ we consider the uncertain actuation, and the additional term $\boldsymbol{\zeta}_\omega$ allows for an unknown time-varying, piecewise-continuous and bounded disturbance affecting the rotational dynamics.

With reference to (4), the translational movement of the quadrotor is influenced by $\dot{T}$ and consequently by the second time derivative $\ddot{T}$ as well. Without a dynamic plant extension for the thrust magnitude, one cannot access the derivatives $\dot{T}$ and $\ddot{T}$. Thus many control designs use a dynamic plant extension for the thrust command. Even though this is not necessary for the backstepping design [6], the dynamic plant extension is still useful to obtain a smooth and less aggressive behavior [5]. Hence we extend the model by two integrators for the thrust magnitude and choose

$$\dddot{T} = u_T \tag{6}$$

as the fourth control input.

In summary, the system's states comprise the position $\mathbf{x}$, the velocity $\boldsymbol{v}$, the attitude $\mathbf{R}$, the angular velocity $\boldsymbol{\omega}$ and the additional states T and $\dot{T}$. We assume all states to be known for the control design and we additionally use the measured acceleration $\dot{\boldsymbol{v}}$.

III. Adaptive Trajectory Tracking Control

With the model derived above, we develop the adaptive trajectory tracking controller in this section. For ease of presentation, we omit the arguments of $\mathbf{M}(\mathbf{R}, T)$ in this section.

A. Backstepping design

As a first step, we define the position tracking error $\mathbf{z}_x = \mathbf{x} - \mathbf{x}_T$, with $\mathbf{x}_T$ being the desired trajectory, and choose the Lyapunov function $V_x = \frac{1}{2}\mathbf{z}_x'\mathbf{z}_x$ to stabilize the origin $\mathbf{z}_x = 0$. The time derivative of V_x is

$$\dot{V}_x = \mathbf{z}_x'(\boldsymbol{v} - \dot{\mathbf{x}}_T) \,, \tag{7}$$

which leads to the desired velocity

$$\boldsymbol{v}_d = \dot{\mathbf{x}}_T + \mathbf{A}_x\mathbf{z}_x \,, \tag{8}$$

with $\mathbf{A}_x < 0$, that drives $V_x \to 0$. The corresponding error dynamics are

$$\dot{\mathbf{z}}_x = \boldsymbol{v} - \dot{\mathbf{x}}_T = \mathbf{A}_x\, \mathbf{z}_x + \mathbf{z}_v \tag{9}$$

with the velocity error defined as $\mathbf{z}_v = \boldsymbol{v} - \boldsymbol{v}_d$. Thus $\dot{V}_x$ actually reads

$$\dot{V}_x = \mathbf{z}_x' \mathbf{A}_x \mathbf{z}_x + \mathbf{z}_x' \mathbf{z}_v \; . \tag{10}$$

Consequently, we want to drive $\mathbf{z}_v \to 0$ and therefore we extend V_x in the following way

$$V_v = V_x + \frac{1}{2} \mathbf{z}_v' \mathbf{z}_v \tag{11}$$

and obtain

$$\dot{V}_v = \mathbf{z}_x' \mathbf{A}_x \mathbf{z}_x + \mathbf{z}_v' (\mathbf{z}_x + \dot{\boldsymbol{v}} - \dot{\boldsymbol{v}}_d) \; . \tag{12}$$

For the desired acceleration, $\dot{\boldsymbol{v}}_d = \ddot{\mathbf{x}}_T + \mathbf{A}_x(\boldsymbol{v} - \dot{\mathbf{x}}_T)$ holds, and $\dot{\boldsymbol{v}}$ in (12) can be influenced by the thrust vector $\mathbf{T}$, see (2). In order to account for the uncertainties in (2), we write the error dynamics for $\mathbf{z}_v$, according to the L1 adaptive control approach, in the following way

$$\dot{\mathbf{z}}_v = \dot{\boldsymbol{v}} - \dot{\boldsymbol{v}}_d = \mathbf{A}_v \mathbf{z}_v - \mathbf{z}_x + \hat{\kappa}_v \mathbf{z}_t + \kappa_v \mathbf{T}_d + \boldsymbol{\sigma}_v \; , \tag{13}$$

with $\mathbf{z}_t = \mathbf{T} - \mathbf{T}_d$, $\mathbf{A}_v < 0$ and $\hat{\kappa}_v$ as an estimate for κ_v. All uncertainties, except the input gain κ_v, are contained in $\boldsymbol{\sigma}_v$, which reads

$$\boldsymbol{\sigma}_v = \mathbf{f}(\boldsymbol{v}) + \mathbf{g} + \boldsymbol{\zeta}_v - \dot{\boldsymbol{v}}_d - \mathbf{A}_v \mathbf{z}_v + \mathbf{z}_x - \tilde{\kappa}_v \mathbf{z}_t \; , \tag{14}$$

with $\tilde{\kappa}_v = \hat{\kappa}_v - \kappa_v$. A state predictor, yet to be defined, will estimate the value for $\boldsymbol{\sigma}_v$, which we denote by $\hat{\boldsymbol{\sigma}}_v$. Our goal is to drive V_v to zero and hence we actually desire $\kappa_v \mathbf{T}_d = \boldsymbol{\sigma}_v$. However, we only know the estimate $\hat{\boldsymbol{\sigma}}_v$; thus $\kappa_v \mathbf{T}_d = \hat{\boldsymbol{\sigma}}_v$ is a more realistic desire. Moreover, we intend to solely compensate for uncertainties in a lower frequency range, hence we assign the desired thrust vector, implicitly in the frequency domain, as

$$\mathbf{T}_d(s) = -d_v(s) \left(\hat{\kappa}_v \mathbf{T}_d(s) + \hat{\boldsymbol{\sigma}}_v(s) \right) \; . \tag{15}$$

This defines an implicit low-pass filter as a transfer function from $\hat{\boldsymbol{\sigma}}_v(s)$ to $\mathbf{T}_d(s)$ with the initial states of the filter set to zero. We use the scalar function $d_v(s)$ to realize a third-order filter and to tune the filter frequencies. The desired thrust can be written explicitly as

$$\begin{aligned} \mathbf{T}_d(s) &= -\hat{\kappa}_v^{-1} \hat{\mathbf{C}}_v(s)\, \hat{\boldsymbol{\sigma}}_v(s) \\ &= -\kappa_v^{-1} \mathbf{C}_v(s) \left[\hat{\boldsymbol{\sigma}}_v(s) + \tilde{\kappa}_v \mathbf{T}_d(s) \right] \\ &=: -\kappa_v^{-1} \hat{\boldsymbol{\eta}}_v(s) \, , \end{aligned} \tag{16}$$

where the low-pass filters $\hat{\mathbf{C}}_v(s)$ and $\mathbf{C}_v(s)$ are given by

$$\hat{\mathbf{C}}_v(s) = \hat{\kappa}_v d_v(s) (\mathbf{I}_{3\times 3} + d_v(s) \hat{\kappa}_v)^{-1} \, , \tag{17}$$

$$\mathbf{C}_v(s) = \kappa_v d_v(s) (\mathbf{I}_{3\times 3} + d_v(s) \kappa_v)^{-1} \, . \tag{18}$$

Using (16), we rewrite (13) as

$$\dot{\mathbf{z}}_v = \dot{\boldsymbol{v}} - \dot{\boldsymbol{v}}_d = \mathbf{A}_v \mathbf{z}_v - \mathbf{z}_x + \hat{\kappa}_v \mathbf{z}_t + \boldsymbol{\sigma}_v - \hat{\boldsymbol{\eta}}_v \, , \tag{19}$$

and (12) as

$$\dot{V}_v = \mathbf{z}_x' \mathbf{A}_x \mathbf{z}_x + \mathbf{z}_v' \mathbf{A}_v \mathbf{z}_v + \hat{\kappa}_v \mathbf{z}_v' \mathbf{z}_t + \mathbf{z}_v' (\boldsymbol{\sigma}_v - \hat{\boldsymbol{\eta}}_v) \; . \tag{20}$$

In the next step, we want to drive $\mathbf{z}_t \to 0$ and extend V_v as follows

$$V_t = V_v + \frac{1}{2} \mathbf{z}_t' \mathbf{z}_t \; . \tag{21}$$

The derivative $\dot{V}_t$ is

$$\begin{aligned} \dot{V}_t = {} & \mathbf{z}_x' \mathbf{A}_x \mathbf{z}_x + \mathbf{z}_v' \mathbf{A}_v \mathbf{z}_v + \mathbf{z}_t' \left(\hat{\kappa}_v \, \mathbf{z}_v + \dot{\mathbf{T}} - \dot{\mathbf{T}}_d \right) \\ & + \mathbf{z}_v' (\boldsymbol{\sigma}_v - \hat{\boldsymbol{\eta}}_v) \; . \end{aligned} \tag{22}$$

As given in (4), $\dot{\mathbf{T}}$ can be influenced by a variation of $\boldsymbol{\omega}_{xy}$ and $\dot{T}$. Since we want to drive $V_t \to 0$, we assign

$$\begin{bmatrix} \boldsymbol{\omega}_{xyd} & \dot{T}_d \end{bmatrix}' = \mathbf{M}^{-1} \left(\dot{\mathbf{T}}_d + \mathbf{A}_t \, \mathbf{z}_t - \hat{\kappa}_v \, \mathbf{z}_v \right) \; , \tag{23}$$

with $\mathbf{A}_t < 0$ and the desired thrust derivate according to (16)

$$\dot{\mathbf{T}}_d(s) = -\hat{\kappa}_v^{-1} \, s \, \hat{\mathbf{C}}_v(s) \, \hat{\boldsymbol{\sigma}}_v(s) \, . \tag{24}$$

Remark 1: Note that $\mathbf{M}^{-1} = \begin{bmatrix} \frac{1}{T}\mathbf{e}_{z1} & \frac{1}{T}\mathbf{e}_{z2} & \mathbf{e}_z \end{bmatrix} \mathbf{R}'$ holds, see (4). Thus we need to ensure that $T \geq T_{\min} > 0$ holds, which is a common obstacle that all quadrotor position tracking controllers have to deal with. To remedy this obstacle, we carefully choose a bounded and sufficiently smooth trajectory such that it is feasible to assume in the case of moderate tracking errors: $T_{\max} \geq T \geq T_{\min} > 0$.

Similar to the previous steps, with the definition of the angular velocity error $\mathbf{z}_r = \begin{bmatrix} \boldsymbol{\omega}_{xy}' - \boldsymbol{\omega}_{xyd}' & \dot{T} - \dot{T}_d \end{bmatrix}'$, we obtain the following error dynamics for $\mathbf{z}_t$

$$\dot{\mathbf{z}}_t = \dot{\mathbf{T}} - \dot{\mathbf{T}}_d = \mathbf{A}_t \mathbf{z}_t + \mathbf{M}\, \mathbf{z}_r - \hat{\kappa}_v \mathbf{z}_v \, . \tag{25}$$

We combine (25) with (22), which results in

$$\dot{V}_t = \mathbf{z}_x' \mathbf{A}_x \mathbf{z}_x + \mathbf{z}_v' \mathbf{A}_v \mathbf{z}_v + \mathbf{z}_t' \mathbf{A}_t \mathbf{z}_t + \mathbf{z}_t' \, \mathbf{M}\, \mathbf{z}_r \tag{26}$$

$$+ \mathbf{z}_v' (\boldsymbol{\sigma}_v - \hat{\boldsymbol{\eta}}_v) \; . \tag{27}$$

In the next step, we extend V_t once more in such a way that

$$V_\omega = V_t + \frac{1}{2} \mathbf{z}_r{}' \mathbf{z}_r \; , \tag{28}$$

in order to achieve $\mathbf{z}_r \to 0$. The time derivative $\dot{V}_\omega$ is

$$\begin{aligned} \dot{V}_\omega = {} & \mathbf{z}_x' \mathbf{A}_x \mathbf{z}_x + \mathbf{z}_v' \mathbf{A}_v \mathbf{z}_v + \mathbf{z}_t' \mathbf{A}_t \mathbf{z}_t + \mathbf{z}_v' (\boldsymbol{\sigma}_v - \hat{\boldsymbol{\eta}}_v) \\ & + \mathbf{z}_r{}' \left(\mathbf{M}'\, \mathbf{z}_t + \begin{bmatrix} \dot{\boldsymbol{\omega}}_{xy}' - \dot{\boldsymbol{\omega}}_{xyd}' & \ddot{T} - \ddot{T}_d \end{bmatrix}' \right) \; . \end{aligned} \tag{29}$$

In order to realize $\ddot{T} = \ddot{T}_d$, we use u_T from (6) as a control input. To realize the desired angular acceleration $\dot{\boldsymbol{\omega}}_{xyd}$, we assign a virtual variable $\bar{\boldsymbol{\tau}}_{xy}$, which we will generate using the torque inputs. Consequently we choose, with $\mathbf{A}_r < 0$,

$$\begin{bmatrix} \bar{\boldsymbol{\tau}}_{xy}' & u_T \end{bmatrix}' = \begin{bmatrix} \dot{\boldsymbol{\omega}}_{xyd}' & \ddot{T}_d \end{bmatrix}' + \mathbf{A}_r \, \mathbf{z}_r - \mathbf{M}'\, \mathbf{z}_t \; . \tag{30}$$

The desired derivatives in (30) read $\begin{bmatrix} \dot{\boldsymbol{\omega}}_{xyd}' & \ddot{T}_d \end{bmatrix}' = \dot{\mathbf{M}}^{-1} \mathbf{M} \begin{bmatrix} \boldsymbol{\omega}_{xyd}' & \dot{T}_d \end{bmatrix}' + \mathbf{M}^{-1} (\ddot{\mathbf{T}}_d + \mathbf{A}_t \dot{\mathbf{z}}_t - \hat{\kappa}_v \dot{\mathbf{z}}_v)$, where $\ddot{\mathbf{T}}_d = -\hat{\kappa}_v^{-1} s^2 \hat{\mathbf{C}}_v(s)\, \hat{\boldsymbol{\sigma}}_v(s)$. The calculation of $\dot{\mathbf{M}}^{-1}$ is straightforward and is omitted due to limited space.

At this stage, we address the control of the heading dynamics. We design a rate controller in order to realize a desired constant angular rate ω_{zd}. This is a suitable choice, since ω_z has no influence on the position tracking control. To that end, we define the angular rate error $z_{\omega z} = \omega_z - \omega_{zd}$ and a virtual variable $\bar{\tau}_z$ and desire, with $a_{\omega z} < 0$,

$$\dot{z}_{\omega z} = \dot{\omega}_z \stackrel{!}{=} \bar{\tau}_z := a_{\omega z}\, z_{\omega z}\ . \tag{31}$$

In order to generate both $\bar{\boldsymbol{\tau}}_{xy}$ from (30) and $\bar{\tau}_z$ from (31) in spite of all uncertainties, we write (5) as

$$\dot{\boldsymbol{\omega}} = \bar{\boldsymbol{\tau}} + \boldsymbol{\kappa}_\omega \boldsymbol{\tau} + \boldsymbol{\sigma}_\omega\,, \tag{32}$$

where $\bar{\boldsymbol{\tau}} = \begin{bmatrix}\bar{\boldsymbol{\tau}}'_{xy} & \bar{\tau}_z\end{bmatrix}'$ holds and $\boldsymbol{\sigma}_\omega$ carries all uncertain values except the input gain matrix $\boldsymbol{\kappa}_\omega$ and reads

$$\boldsymbol{\sigma}_\omega = \mathbf{J}^{-1}(\mathbf{J}\boldsymbol{\omega}\times\boldsymbol{\omega}) + \boldsymbol{\zeta}_\omega - \bar{\boldsymbol{\tau}}\,. \tag{33}$$

Similar to the definition of the desired thrust in (15), we choose the control torques to be

$$\boldsymbol{\tau}(s) = -d_\omega(s)(\hat{\boldsymbol{\kappa}}_\omega \boldsymbol{\tau}(s) + \hat{\boldsymbol{\sigma}}_\omega(s))\,, \tag{34}$$

which can be written explicitly, with $\tilde{\boldsymbol{\kappa}}_\omega = \hat{\boldsymbol{\kappa}}_\omega - \boldsymbol{\kappa}_\omega$, as

$$\begin{aligned}\boldsymbol{\tau}(s) &= -\hat{\boldsymbol{\kappa}}_\omega^{-1}\hat{\mathbf{C}}_\omega(s)\,\hat{\boldsymbol{\sigma}}_\omega(s) \\ &= -\boldsymbol{\kappa}_\omega^{-1}\mathbf{C}_\omega(s)[\hat{\boldsymbol{\sigma}}_\omega(s) + \tilde{\boldsymbol{\kappa}}_\omega\boldsymbol{\tau}(s)] \\ &=: -\boldsymbol{\kappa}_\omega^{-1}\hat{\boldsymbol{\eta}}_\omega(s)\,.\end{aligned} \tag{35}$$

The low-pass filters $\hat{\mathbf{C}}_\omega(s)$ and $\mathbf{C}_\omega(s)$ read

$$\hat{\mathbf{C}}_\omega(s) = \hat{\boldsymbol{\kappa}}_\omega d_\omega(s)(\mathbf{I}_{3\times3} + d_\omega(s)\hat{\boldsymbol{\kappa}}_\omega)^{-1}\,, \tag{36}$$

$$\mathbf{C}_\omega(s) = \boldsymbol{\kappa}_\omega d_\omega(s)(\mathbf{I}_{3\times3} + d_\omega(s)\boldsymbol{\kappa}_\omega)^{-1}\,. \tag{37}$$

The torque $\boldsymbol{\tau}$ assigned in (35) and u_T assigned in (30) form the control law for the extended plant model. The estimates $\hat{\boldsymbol{\sigma}}_v$, $\hat{\boldsymbol{\sigma}}_\omega$ therein are going to be defined by the adaptation algorithm in Sec. III-F below. In order to analyze the transient behavior of the closed-loop error system, we proceed and rewrite (32) using (35) as

$$\dot{\boldsymbol{\omega}} = \bar{\boldsymbol{\tau}} + \boldsymbol{\sigma}_\omega - \hat{\boldsymbol{\eta}}_\omega \tag{38}$$

and obtain the following error dynamics

$$\dot{\mathbf{z}}_r = \mathbf{A}_r\mathbf{z}_r - \mathbf{M}'\mathbf{z}_t + \mathbf{B}_r(\boldsymbol{\sigma}_\omega - \hat{\boldsymbol{\eta}}_\omega)\,, \tag{39}$$

with $\mathbf{B}_r = \mathrm{diag}(1,1,0)$, and

$$\dot{z}_{\omega z} = a_{\omega z} z_{\omega z} + \mathbf{b}'_\varphi(\boldsymbol{\sigma}_\omega - \hat{\boldsymbol{\eta}}_\omega) \tag{40}$$

with $\mathbf{b}'_\varphi = [0\ 0\ 1]'$. For the Lyapunov function V, which contains all relevant states and is defined as

$$V = V_\omega + \frac{1}{2}{z_{\omega z}}^2\,, \tag{41}$$

$\dot{V}$ takes the form

$$\begin{aligned}\dot{V} = {}& \mathbf{z}'_x\mathbf{A}_x\mathbf{z}_x + \mathbf{z}'_v\mathbf{A}_v\mathbf{z}_v + \mathbf{z}'_t\mathbf{A}_t\mathbf{z}_t + {\mathbf{z}_r}'\mathbf{A}_r\mathbf{z}_r + \\ & \mathbf{z}'_v(\boldsymbol{\sigma}_v - \hat{\boldsymbol{\eta}}_v) + \mathbf{z}'_r\mathbf{B}_r(\boldsymbol{\sigma}_\omega - \hat{\boldsymbol{\eta}}_\omega) \\ & + a_{\omega z}{z_{\omega z}}^2 + z_{\omega z}\mathbf{b}'_\varphi(\boldsymbol{\sigma}_\omega - \hat{\boldsymbol{\eta}}_\omega)\,.\end{aligned} \tag{42}$$

If we had perfect estimation in the whole frequency domain, i.e. $\boldsymbol{\sigma}_v = \hat{\boldsymbol{\eta}}_v$ and $\boldsymbol{\sigma}_\omega = \hat{\boldsymbol{\eta}}_\omega$, (42) would be negative definite and the closed-loop system asymptotically stable. But since we intend to solely compensate for uncertainties in a certain frequency range and since a small estimation error will always remain, further analysis is needed.

B. Nonlinear time-varying error dynamics

By means of the backstepping design in the previous section, we obtain the following time-varying error dynamics. With the error state vector defined as $\mathbf{z}' = [\mathbf{z}'_x, \mathbf{z}'_v, \mathbf{z}'_t, \mathbf{z}'_r, z_{\omega z}]'$, we write (9), (19), (25), (39) and (40) as

$$\dot{\mathbf{z}} = \begin{bmatrix}\mathbf{A}_x & \mathbf{I}_{3\times3} & \mathbf{0}_{3\times3} & \mathbf{0}_{3\times3} & \mathbf{0}_{3\times1}\\ -\mathbf{I}_{3\times3} & \mathbf{A}_v & \hat{\kappa}_v\cdot\mathbf{I}_{3\times3} & \mathbf{0}_{3\times3} & \mathbf{0}_{3\times1}\\ \mathbf{0}_{3\times3} & -\hat{\kappa}_v\cdot\mathbf{I}_{3\times3} & \mathbf{A}_t & \mathbf{M}_H & \mathbf{0}_{3\times1}\\ \mathbf{0}_{3\times3} & \mathbf{0}_{3\times3} & -\mathbf{M}'_H & \mathbf{A}_r & \mathbf{0}_{3\times1}\\ \mathbf{0}_{1\times3} & \mathbf{0}_{1\times3} & \mathbf{0}_{1\times3} & \mathbf{0}_{1\times3} & a_{\omega z}\end{bmatrix}\mathbf{z} \tag{43}$$

$$\begin{aligned}&+ \begin{bmatrix}\mathbf{0}_{3\times6}\\ \mathbf{0}_{3\times6}\\ \mathbf{I}_{6\times6}\\ \mathbf{0}_{1\times6}\end{bmatrix}\begin{bmatrix}\mathbf{M}_\Delta\,\mathbf{z}_r\\ -\mathbf{M}'_\Delta\mathbf{z}_t\end{bmatrix} + \begin{bmatrix}\mathbf{0}_{3\times3} & \mathbf{0}_{3\times3}\\ \mathbf{I}_{3\times3} & \mathbf{0}_{3\times3}\\ \mathbf{0}_{3\times3} & \mathbf{0}_{3\times3}\\ \mathbf{0}_{3\times3} & \mathbf{B}_r\\ \mathbf{0}_{1\times3} & \mathbf{b}'_\varphi\end{bmatrix}\begin{bmatrix}\boldsymbol{\sigma}_v - \hat{\boldsymbol{\eta}}_v\\ \boldsymbol{\sigma}_\omega - \hat{\boldsymbol{\eta}}_\omega\end{bmatrix}\\ &=: \mathbf{A}\mathbf{z} + \mathbf{B}_f\mathbf{f} + \mathbf{B}(\boldsymbol{\sigma} - \hat{\boldsymbol{\eta}})\,,\end{aligned}$$

with $\boldsymbol{\sigma} = \begin{bmatrix}\boldsymbol{\sigma}'_v, \boldsymbol{\sigma}'_\omega\end{bmatrix}'$, $\mathbf{f} = [(\mathbf{M}_\Delta\,\mathbf{z}_r)', (-\mathbf{M}'_\Delta\mathbf{z}_t)']'$ and $\hat{\boldsymbol{\eta}}(s) = \begin{bmatrix}\hat{\boldsymbol{\eta}}_v(s)', \hat{\boldsymbol{\eta}}_\omega(s)'\end{bmatrix}' = \mathbf{C}(s)[\hat{\boldsymbol{\sigma}}(s) + \tilde{\boldsymbol{\kappa}}\mathbf{u}(s)]$, where $\mathbf{C}(s) = \mathrm{diag}(\mathbf{C}_v(s), \mathbf{C}_\omega(s))$, $\tilde{\boldsymbol{\kappa}} = \mathrm{diag}(\tilde{\kappa}_v\cdot\mathbf{I}_{3\times3}, \tilde{\boldsymbol{\kappa}}_\omega)$ and $\mathbf{u} = \begin{bmatrix}\mathbf{T}'_d & \boldsymbol{\tau}'\end{bmatrix}'$. In (43), we split the nonlinear function $\mathbf{M}(\mathbf{R}, T)$ into two parts, such that $\mathbf{M}(\mathbf{R}, T) = \mathbf{M}_H + \mathbf{M}_\Delta(\mathbf{R}, T)$ holds. $\mathbf{M}_H$ is a constant matrix containing the values that $\mathbf{M}(\mathbf{R}, T)$ has during hovering. Thus for maneuvers near hovering, $\mathbf{M}_\Delta$ is quite small. The error dynamics comprise a linear part $\mathbf{A}\mathbf{z}$, where $\mathbf{A}$ is Hurwitz, and two nonlinear and time-varying functions $\mathbf{B}_f\mathbf{f}$ and $\mathbf{B}(\boldsymbol{\sigma} - \hat{\boldsymbol{\eta}})$. For the latter,

$$\boldsymbol{\sigma} - \hat{\boldsymbol{\eta}} = \mathfrak{L}^{-1}[(\mathbf{I} - \mathbf{C}(s))\hat{\boldsymbol{\sigma}}(s) - \tilde{\boldsymbol{\sigma}} - \mathbf{C}(s)\tilde{\boldsymbol{\kappa}}\mathbf{u}(s)] \tag{44}$$

holds and $\mathfrak{L}^{-1}[.]$ denotes the inverse Laplace transformation from the frequency domain back into the time domain. Thus the function $\boldsymbol{\sigma} - \hat{\boldsymbol{\eta}}$ consists of three parts: All high frequency excitations in $\hat{\boldsymbol{\sigma}}$ that pass the high-pass filter $\mathbf{I} - \mathbf{C}(s)$, the estimation error $\tilde{\boldsymbol{\sigma}} = \hat{\boldsymbol{\sigma}} - \boldsymbol{\sigma}$ and an excitation within the low-pass filter frequencies of $\mathbf{C}(s)$ caused by an input gain mismatch $\tilde{\boldsymbol{\kappa}}\mathbf{u}(s)$.

Both functions, $\boldsymbol{\sigma} = \boldsymbol{\sigma}(t, \mathbf{z})$ and $\mathbf{f} = \mathbf{f}(t, \mathbf{z})$, depend on the desired trajectory and the error states. Since we track a sufficiently smooth and bounded trajectory, more precisely by choosing $\mathbf{x}_T \in C^4$, we can state the following properties needed for the L1 adaptive control design [16, Ch. 3.3]:

1) Boundedness of $\boldsymbol{\sigma}(t, \mathbf{0})$ and $\mathbf{f}(t, \mathbf{0})$: There exists $b > 0$, such that $\|\boldsymbol{\sigma}(t, \mathbf{0})\|_\infty \leq b$ and $\mathbf{f}(t, \mathbf{0}) = 0$ holds $\forall t \geq 0$.

2) Semiglobal Lipschitz condition for $\boldsymbol{\sigma}(t, \mathbf{z})$ and $\mathbf{f}(t, \mathbf{z})$: For arbitrary $\delta > 0$, there exist positive constants $K_{\boldsymbol{\sigma}}(\delta) > 0$ and $K_{\mathbf{f}}(\delta) > 0$ uniformly in time, such that for all

$\|\mathbf{z}_i\|_\infty \leq \delta,\ i = 1, 2$

$$\|\boldsymbol{\sigma}(t, \mathbf{z}_1) - \boldsymbol{\sigma}(t, \mathbf{z}_2)\|_\infty \leq K_{\boldsymbol{\sigma}}(\delta) \|\mathbf{z}_1 - \mathbf{z}_2\|_\infty , \quad (45)$$

$$\|\mathbf{f}(t, \mathbf{z}_1) - \mathbf{f}(t, \mathbf{z}_2)\|_\infty \leq K_{\mathbf{f}}(\delta) \|\mathbf{z}_1 - \mathbf{z}_2\|_\infty . \quad (46)$$

The inequality (46) holds since we assume $T \geq T_{\min} > 0$, see Remark 1.

3) Semiglobal uniform boundedness of $\boldsymbol{\sigma}(t, \mathbf{z})$ and $\mathbf{f}(t, \mathbf{z})$: For every $\delta > 0$, let L_δ be defined as

$$L_\delta := \frac{\bar{\delta}(\delta)}{\delta} \max\{K_{\boldsymbol{\sigma}}(\bar{\delta}(\delta)),\ K_{\mathbf{f}}(\bar{\delta}(\delta))\} , \quad (47)$$

with $\bar{\delta}(\delta) := \delta + \bar{\gamma}_1$, where $\bar{\gamma}_1$ is an arbitrary small positive constant. Then, an upper bound for $\boldsymbol{\sigma}(t, \mathbf{z})$, for all $t \in [0, t_b]$ with an arbitrary $t_b < \infty$ and $\|\mathbf{z}(t)\|_{\mathcal{L}_\infty} \leq \rho$, is given by

$$\|\boldsymbol{\sigma}(t, \mathbf{z})\|_{\mathcal{L}_\infty} \leq L_\rho \, \rho + b \quad (48)$$

with b from Sec. III-B.1 above and for $\mathbf{f}(t, \mathbf{z})$

$$\|\mathbf{f}(t, \mathbf{z})\|_{\mathcal{L}_\infty} \leq L_\rho \, \rho < L_\rho \, \rho + b \, . \quad (49)$$

See [16, Ch. A.8] for more details on the existence of these bounds. Furthermore, we have the following properties of the error dynamics:

4) Bounded solution to the initial value problem: Let $\mathbf{z}_{\text{in}}$ be the solution for the initial value problem:

$$\dot{\mathbf{z}} = \mathbf{A}\, \mathbf{z} \, , \quad \mathbf{z}(t{=}0) = \mathbf{z}_0 \, , \quad \|\mathbf{z}_0\|_\infty \leq \rho_0 \, . \quad (50)$$

Then $\mathbf{z}_{\text{in}}$ is upper bounded by

$$\|\mathbf{z}_{\text{in}}\|_{\mathcal{L}_\infty} \leq \|s\mathbf{H}(s)\|_{\mathcal{L}_1} \rho_0 = \rho_{\text{in}} \quad (51)$$

with $\mathbf{H}(s) = (s\mathbf{I} - \mathbf{A})^{-1}$.

5) Partial knowledge of the system input gain: For the nominal system input, $\hat{\boldsymbol{\kappa}} = \text{diag}(\hat{m}^{-1} \cdot \mathbf{I}_{3\times 3}, \hat{\mathbf{J}}^{-1})$ holds. Since the uncertain mass m and inertia $\mathbf{J}$ is positive and physically bounded away from zero, $\boldsymbol{\kappa}$ is nonsingular and $\text{sgn}(\kappa_{ii}) = +1$. Furthermore, $\hat{\kappa}_{ij} = 0$ holds with $i \neq j$, thus it is reasonable to assume that $\boldsymbol{\kappa}$ stays strictly row-diagonally dominant despite moderate uncertainties. In addition, we assume there exists a compact and convex set K, such that $\boldsymbol{\kappa} \in K$ holds and we can determine an upper bound $\max_{\boldsymbol{\kappa} \in K} \{\|\boldsymbol{\kappa} - \hat{\boldsymbol{\kappa}}\|_2\} = \tilde{\kappa}_{max}$.

In the following sections, we first define a reference system, which we intend to realize with our error system (43). We derive a sufficient stability condition and upper bounds for the error states of the reference system and the reference control inputs. Then we define a state predictor and an adaptation law to estimate the uncertainties. With the knowledge of the estimation error, we can subsequently derive upper bounds for the states of the error dynamics and for the control signals. The whole closed-loop is shown in Fig. 2. Note that the reference model solely serves for analysis purposes and is not implemented in the controller.

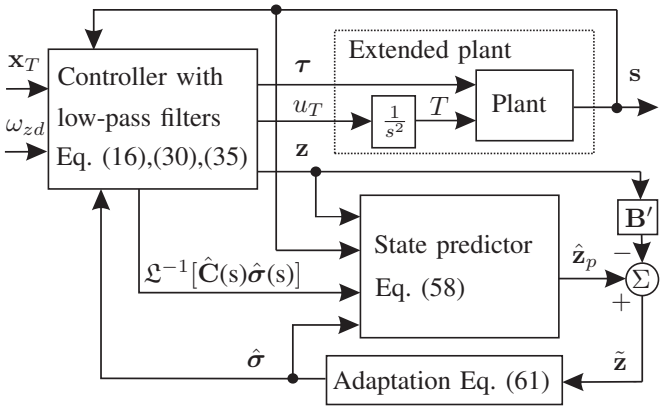

Fig. 2. Complete closed-loop structure with $\mathbf{x}_T$ and ω_{zd} as the desired position trajectory and angular rate and $\mathbf{s} = \{\mathbf{x}, \boldsymbol{v}, \dot{\boldsymbol{v}}, \mathbf{R}, \boldsymbol{\omega}, T, \dot{T}\}$ are all states and measurements necessary for control.

C. Reference model and sufficient condition for stability

The reference model has the same structure as (43) and is given by

$$\dot{\mathbf{z}}_{\text{ref}} = \mathbf{A}\mathbf{z}_{\text{ref}} + \mathbf{B}_f \mathbf{f}_{\text{ref}} + \mathbf{B}(\boldsymbol{\sigma}_{\text{ref}} - \boldsymbol{\eta}_{\text{ref}}) \, . \quad (52)$$

The reference model characterizes the desired system dynamics and to this end, perfect estimation is assumed: $\boldsymbol{\eta}_{\text{ref}}(s) = \mathbf{C}(s)\boldsymbol{\sigma}_{\text{ref}}(s)$. Moreover, $\mathbf{z}_{\text{ref}}(0) = \mathbf{z}_0$ holds. Note that (52) is a closed-loop system, thus $\mathbf{u}_{\text{ref}} = \begin{bmatrix} \mathbf{T}'_{\text{d,ref}} & \boldsymbol{\tau}'_{\text{ref}} \end{bmatrix}'$ is an internal signal of the reference model and does not explicitly appear in (52). Due to the nonlinear function $\mathbf{B}_f \mathbf{f}_{\text{ref}}$, our reference model differs from the reference model structure used in the L1 adaptive control approach for linear reference systems [16]. We nevertheless use the design approach for linear reference systems in such a way that we solely rely on the stabilizing property of the linear part $\mathbf{A}\mathbf{z}_{\text{ref}}$ and treat $\mathbf{B}_f \mathbf{f}_{\text{ref}}$ as additional external signal. This may render our condition for stability in Lemma 1 below slightly conservative, but we preserve the well-understood theory for the most part and keep the analysis tight. However, we experienced in simulations that $\mathbf{B}_f \mathbf{f}_{\text{ref}}$ has a rather small influence on the stability condition when moderate trajectories are tracked.

Lemma 1: For the reference system, given in (52), if there exists $\rho_r > \rho_{\text{in}}$, for a given ρ_0, and a corresponding L_{ρ_r}, as defined in (47), such that

$$\|\mathbf{G}(s)\|_{\mathcal{L}_1} + \|\mathbf{H}(s)\mathbf{B}_f\|_{\mathcal{L}_1} < \frac{\rho_r - \rho_{\text{in}}}{L_{\rho r}\rho_r + b} \, , \quad (53)$$

where $\mathbf{G}(s) = \mathbf{H}(s)\mathbf{B}(\mathbf{I} - \mathbf{C}(s))$, then

$$\|\mathbf{z}_{\text{ref}}\|_{\mathcal{L}_\infty} < \rho_r \, , \quad (54)$$

$$\|\mathbf{u}_{\text{ref}}\|_{\mathcal{L}_\infty} < \rho_{ur} \quad \text{with} \quad (55)$$

$$\rho_{ur} := \|\boldsymbol{\kappa}^{-1}\mathbf{C}(s)\|_{\mathcal{L}_1}(L_{\rho r}\rho_r + b) \, . \quad (56)$$

The proof is given in the appendix.

Remark 2: Due to the bounds (54) and (55), we know that the reference control input for the extended plant model $u_{T,\text{ref}}$, which is included in (52), is also bounded. But because of limited space, we do not derive this bound.

Remark 3: In order to fulfill condition (53) for a given ρ_{in}, we can first choose a value for ρ_r and then use $d_v(s)$,

$d_\omega(s)$ and the eigenvalues of $\mathbf{A}$ to adjust $\|\mathbf{G}(s)\|_{\mathcal{L}_1}$ and $\|\mathbf{H}(s)\mathbf{B}_f\|_{\mathcal{L}_1}$ accordingly. With a high value for ρ_r, we can realize small eigenvalues of $\mathbf{A}$ and low cutoff frequencies of $\mathbf{C}(s)$ to fulfill the condition. In turn, for ρ_r arbitrarily close to ρ_{in}, we need fast eigenvalues and even higher cutoff frequencies to ensure stability. Although the latter yields higher performance, one sacrifices robustness compared to the former adjustment [16]. Thus the design of ρ_r, $\mathbf{H}(s)$ and $\mathbf{C}(s)$, poses a trade-off between performance and robustness.

Remark 4: For the derivation of L_{ρ_r} in (53), one needs to choose a value for $\bar{\gamma}_1$, see (47). Together with ρ_r, the value ρ defined as

$$\rho := \rho_r + \bar{\gamma}_1 \,, \tag{57}$$

is going to be the upper bound for $\|\mathbf{z}\|_{\mathcal{L}_\infty}$, which is shown in the proceeding analysis. The value $\bar{\gamma}_1$ can be arbitrarily small, which leads to a better performance but results in a stronger restriction on the estimation error to be achieved. A bigger value for $\bar{\gamma}_1$ in turn poses a weaker restriction on the estimation error but also leads to a weaker performance. But with the adaptation scheme in this work, yet to be defined, the only restriction for choosing a very small $\bar{\gamma}_1$ is the available CPU power.

D. State predictor

In the L1 adaptive control approach, the state predictor has the same structure as the plant model. But since not all system states are directly affected by uncertainties in our application, we solely use those states for the state predictor that are directly affected by the uncertainties $\boldsymbol{\sigma}$. The states that are not directly affected by $\boldsymbol{\sigma}$, we consider as known and replace them with their measured values. Hence the predictor states are $\hat{\mathbf{z}}_p = [\hat{\mathbf{z}}_v', \hat{\mathbf{z}}_{r12}', \hat{z}_{\omega z}]' = \mathbf{B}'\hat{\mathbf{z}} := \mathbf{B}'[\mathbf{z}_x', \hat{\mathbf{z}}_v', \mathbf{z}_t', \hat{\mathbf{z}}_{r12}', z_{r3}, \hat{z}_{\omega z}]'$, where $\mathbf{z}_{r12}$ are the first two entries of $\mathbf{z}_r$ and z_{r3} is the third entry, and the state predictor takes the form

$$\dot{\hat{\mathbf{z}}}_p = \mathbf{B}'\dot{\hat{\mathbf{z}}} = \mathbf{B}'\mathbf{A}\hat{\mathbf{z}} + \mathbf{B}'\mathbf{B}_f\mathbf{f} + \hat{\boldsymbol{\sigma}} - \mathfrak{L}^{-1}[\hat{\mathbf{C}}(s)\hat{\boldsymbol{\sigma}}(s)] \,. \tag{58}$$

Note that for $\mathbf{f} = \mathbf{f}(t, \mathbf{z})$, we also use the measured states $\mathbf{z}$.

E. Estimation error dynamics

To derive the estimation error dynamics, we first rewrite (43) using $\hat{\mathbf{C}}(s)$ instead of $\mathbf{C}(s)$, which reads according to (16) and (35)

$$\dot{\mathbf{z}} = \mathbf{A}\mathbf{z} + \mathbf{B}_f\mathbf{f} + \mathbf{B}(\boldsymbol{\sigma} - \mathfrak{L}^{-1}[\hat{\mathbf{C}}(s)\hat{\boldsymbol{\sigma}}(s)] - \tilde{\boldsymbol{\kappa}}\mathbf{u}) \,. \tag{59}$$

With the state estimation error defined as $\tilde{\mathbf{z}} = \mathbf{B}'(\hat{\mathbf{z}} - \mathbf{z}) = [\tilde{\mathbf{z}}_v', \tilde{\mathbf{z}}_{r12}', \tilde{z}_{\omega z}]'$ and since $\mathbf{B}\tilde{\mathbf{z}} = \hat{\mathbf{z}} - \mathbf{z}$ holds, we obtain the following estimation error dynamics along with (58) and (59)

$$\dot{\tilde{\mathbf{z}}} = \mathbf{A}_e\tilde{\mathbf{z}} + \tilde{\boldsymbol{\sigma}} + \tilde{\boldsymbol{\kappa}}\mathbf{u} \,, \tag{60}$$

where $\mathbf{A}_e = \mathbf{B}'\mathbf{A}\mathbf{B}$.

F. Adaptation law

We decide to use the Piecewise-Constant Adaptation Law presented in [16, Ch. 3.3.] and [17], which is defined for our application as

$$\hat{\boldsymbol{\sigma}} = \hat{\boldsymbol{\sigma}}(iT_s) \,, \quad t \in [iT_s, (i+1)T_s) \,, \tag{61}$$

$$\hat{\boldsymbol{\sigma}}(iT_s) = -\boldsymbol{\Phi}^{-1}(T_s)\boldsymbol{\mu}(iT_s) \,, \tag{62}$$

with $i \in \mathbb{N}_0$ and the adaptation sampling time T_s, where

$$\boldsymbol{\Phi}(T_s) = \mathbf{A}_e^{-1}(\mathbf{e}^{\mathbf{A}_e T_s} - \mathbf{I}) \tag{63}$$

$$\boldsymbol{\mu}(iT_s) = \mathbf{e}^{\mathbf{A}_e T_s}\tilde{\mathbf{z}}(iT_s) \,. \tag{64}$$

The only parameter for adjusting the adaptation speed is the sampling time T_s, which can be arbitrarily small with sufficient CPU power.

G. Transient and Steady-State Performance

In this section, we analyze the transient and steady-state performance of the all-over closed-loop tracking system. To achieve a bounded and stable tracking performance, we first need to choose the positive constants $\bar{\gamma}_0$ and β in

$$\gamma_1 := \frac{\|\mathbf{H}(s)\mathbf{B}\mathbf{C}(s)\mathbf{H}_e^{-1}(s)\|_{\mathcal{L}_1}}{1 - (\|\mathbf{G}(s)\|_{\mathcal{L}_1} + \|\mathbf{H}(s)\mathbf{B}_f\|_{\mathcal{L}_1})\, L_{\rho_r}} \bar{\gamma}_0 + \beta \,, \tag{65}$$

with $\mathbf{H}_e^{-1}(s) := s\mathbf{I} - \mathbf{A}_e$, small enough to ensure $\gamma_1 \leq \bar{\gamma}_1$. Then we must select the adaptation sampling time T_s such that

$$\gamma_0(T_s) < \bar{\gamma}_0 \,. \tag{66}$$

The function $\gamma_0(T_s)$ is defined in [16, Ch. 3.3.] for a more general case that covers our application. Thus we refer the interested reader to the reference. The calculation of $\gamma_0(T_s)$ requires the properties stated in Sec. III-B.5 concerning the partial knowledge of the input gain. The associated Lemma 3.3.1 in [16] proves that $\lim_{T_s \to 0} \gamma_0(T_s) = 0$ holds. With ρ defined in (57) and with $\rho_u := \rho_{ur} + \gamma_2$, where

$$\gamma_2 := \|\boldsymbol{\kappa}^{-1}\mathbf{C}(s)\|_{\mathcal{L}_1} L_{\rho_r}\gamma_1 + \|\boldsymbol{\kappa}^{-1}\mathbf{C}(s)\mathbf{H}_e^{-1}(s)\|_{\mathcal{L}_1}\bar{\gamma}_0 \,, \tag{67}$$

Lemma 3.3.3 in [16] states:

Lemma 2: If (53) and (66) are satisfied and further the bounds $\|\mathbf{z}\|_{\mathcal{L}_\infty^{[0,\tau]}} \leq \rho$ and $\|\mathbf{u}\|_{\mathcal{L}_\infty^{[0,\tau]}} \leq \rho_u$ exist, one has

$$\|\tilde{\mathbf{z}}\|_{\mathcal{L}_\infty^{[0,\tau]}} < \bar{\gamma}_0 \,. \tag{68}$$

The proof is given in [16, Ch. 3.3.].

Remark 5: The existence of the bounds $\|\mathbf{z}\|_{\mathcal{L}_\infty^{[0,\tau]}} \leq \rho$ and $\|\mathbf{u}\|_{\mathcal{L}_\infty^{[0,\tau]}} \leq \rho_u$ has not been proven so far, but is the content of the following theorem.

Theorem 1: Let the adaptation rate be chosen to satisfy (66). Given the error system (43) and the reference system (52), if $\|\mathbf{z}_0\|_\infty \leq \rho_0$, we have

$$\|\mathbf{z}\|_{\mathcal{L}_\infty} \leq \rho \tag{69}$$

$$\|\mathbf{u}\|_{\mathcal{L}_\infty} \leq \rho_u \tag{70}$$

$$\|\tilde{\mathbf{z}}\|_{\mathcal{L}_\infty} \leq \bar{\gamma}_0 \tag{71}$$

$$\|\mathbf{z}_{ref} - \mathbf{z}\|_{\mathcal{L}_\infty} \leq \gamma_1 \tag{72}$$

$$\|\mathbf{u}_{ref} - \mathbf{u}\|_{\mathcal{L}_\infty} \leq \gamma_2 \,. \tag{73}$$

The proof is given in the appendix.

Remark 6: The bounds given in Theorem 1 imply the boundedness of the input signal u_T. Due to limited space we do not derive this bound.

IV. Simulation Results

We analyzed the performance of the presented controller in numerical simulations, where we implemented the plant model from Sec. II with uncertain parameters and time-varying external disturbances given in Tab. I. The chosen parameters for the controller as well as the derived bounds can also be seen in Tab. I.

As we experienced, the theoretical bound $\|\boldsymbol{\sigma}_\omega\|_{\mathcal{L}_\infty}$ is much more conservative than $\|\boldsymbol{\sigma}_v\|_{\mathcal{L}_\infty}$ and $\|\mathbf{f}\|_{\mathcal{L}_\infty}$ due to the extensive calculations necessary for $\boldsymbol{\sigma}_\omega$. In order to avoid a very conservative tuning, which would have caused very high cutoff frequencies and poor robustness, we derived $L_{\rho r}$ and b such that $\|\mathbf{f}\|_{\mathcal{L}_\infty} < \|\boldsymbol{\sigma}_v\|_{\mathcal{L}_\infty} \leq L_{\rho r}\rho_r + b$ held with $\|\mathbf{z}\|_{\mathcal{L}_\infty} \leq \rho$ and assumed $\|\boldsymbol{\sigma}_\omega\|_{\mathcal{L}_\infty} \leq \|\boldsymbol{\sigma}_v\|_{\mathcal{L}_\infty}$. This was reasonable for our simulations, where we obtained $2 \cdot \|\boldsymbol{\sigma}_\omega\|_{\mathcal{L}_\infty} < \|\boldsymbol{\sigma}_v\|_{\mathcal{L}_\infty}$. Further, we chose $d_v(s)$ and $d_\omega(s)$ such that condition (53) was fulfilled with cutoff frequencies of 30 rad/sec for $\hat{\mathbf{C}}_v(s)$ and 100 rad/sec for $\hat{\mathbf{C}}_\omega(s)$. With an adaptation sampling time of $T_s = 10^{-5}$ sec, we met condition (66). The simulation was initialized with $\|\mathbf{z}(0)\|_\infty < 0.3$, which yielded $\rho_{\text{in}} = 0.45$.

Fig. 3 shows the simulation result for the parameter setting in Tab. I. We commanded different set points $\mathbf{x}_\text{C}$ and provided a sufficiently smooth desired trajectory $\mathbf{x}_\text{T} \in C^4$ by way of a linear filter. For a nonadaptive backstepping controller without low-pass filters, i.e. $\mathbf{u} = -\hat{\boldsymbol{\kappa}}^{-1}\hat{\boldsymbol{\sigma}}$, with constant $\hat{\boldsymbol{\sigma}}$ based on the assumed parameters and same eigenvalues of $\mathbf{A}$, we observed a huge deviation from the desired trajectory due to the uncertainties, see $\mathbf{x}_\text{N}$ in Fig. 3. In particular, the time-varying disturbance apparently affected the system to a large extent. With the adaptive controller, shown by $\mathbf{x}_\text{A}$ in Fig. 3, the system tracked the desired trajectory precisely. Even the time-varying disturbance was effectively compensated. In this simulation, we obtained $\|\boldsymbol{\sigma}_v\|_{\mathcal{L}_\infty} < 10.6$, $\|\boldsymbol{\sigma}_\omega\|_{\mathcal{L}_\infty} < 5.2$, $\|\tilde{\mathbf{z}}\|_{\mathcal{L}_\infty} < 2 \cdot 10^{-4}$, $\|\mathbf{f}\|_{\mathcal{L}_\infty} < 0.4$, $\|\mathbf{z}\|_{\mathcal{L}_\infty} < 0.5$ and $\|\mathbf{u}\|_{\mathcal{L}_\infty} < 4.9$, which shows that the actual values are much smaller than the theoretical bounds.

V. Conclusions

The L1 adaptive control approach, applied to a quadrotor helicopter for position tracking, appears to be a promising solution to handle various parameter uncertainties and disturbances. With this controller, we are confident of avoiding costly parameter identifications for our practical application in progress and being able to compensate, for instance, for constant wind and moderate wind gusts. For our application, we slightly modified the L1 adaptive control design to handle the nonlinear error dynamics with the same technique available for linear systems. The recently published L1 adaptive control extension for nonlinear time-varying reference systems [18], which considers systems with single inputs and scalar uncertainty functions, may yield a less conservative stability criterion for our control law, provided the theory is applicable. Therefore we are currently investigating the feasibility and the expected benefit of this new approach for our application.

TABLE I

Controller and plant parameters in SI units.

Controller parameters		
$\mathbf{A}_x = -\mathbf{I}_{3\times3}$	$\mathbf{A}_v = -3 \cdot \mathbf{I}_{3\times3}$	$\mathbf{A}_t = -30 \cdot \mathbf{I}_{3\times3}$
$\mathbf{A}_r = -60 \cdot \mathbf{I}_{3\times3}$	$a_{\omega z} = -3$	$d_v(s) = \frac{18280}{s^3+96s^2+3069s}$
$d_\omega(s) = \frac{56}{s}$	$\|\mathbf{G}(s)\|_{\mathcal{L}_1} \leq 0.136$	$\|\mathbf{H}(s)\mathbf{B}_f\|_{\mathcal{L}_1} = 0.0365$
Uncertain plant parameters and external inputs		
$\mathbf{f}(\boldsymbol{v}) = 2 \cdot \hat{\mathbf{f}}(\boldsymbol{v}) = -\text{diag}(0.36, 0.36, 0.36) \cdot \boldsymbol{v}$		$m = 0.8 \cdot \hat{m} = 0.45$
$\mathbf{J} = 1.4 \cdot \hat{\mathbf{J}} = \text{diag}(6.8, 6.8, 11.2) \cdot 10^{-3}$		$g = \hat{g} = 9.81$
$\hat{\kappa}_v = 1/\hat{m}$	$\kappa_v = 0.78 \cdot \hat{\kappa}_v$	$\hat{\boldsymbol{\kappa}}_\omega = \hat{\mathbf{J}}^{-1}$
$\boldsymbol{\kappa}_{\omega 11} = 0.75 \cdot \hat{\boldsymbol{\kappa}}_{\omega 11}$	$\boldsymbol{\kappa}_{\omega 12} = 0.00 \cdot \hat{\boldsymbol{\kappa}}_{\omega 11}$	$\boldsymbol{\kappa}_{\omega 13} = 0.42 \cdot \hat{\boldsymbol{\kappa}}_{\omega 11}$
$\boldsymbol{\kappa}_{\omega 21} = 0.00 \cdot \hat{\boldsymbol{\kappa}}_{\omega 22}$	$\boldsymbol{\kappa}_{\omega 22} = 0.74 \cdot \hat{\boldsymbol{\kappa}}_{\omega 22}$	$\boldsymbol{\kappa}_{\omega 23} = 0.04 \cdot \hat{\boldsymbol{\kappa}}_{\omega 22}$
$\boldsymbol{\kappa}_{\omega 31} = 0.01 \cdot \hat{\boldsymbol{\kappa}}_{\omega 33}$	$\boldsymbol{\kappa}_{\omega 32} = 0.00 \cdot \hat{\boldsymbol{\kappa}}_{\omega 33}$	$\boldsymbol{\kappa}_{\omega 33} = 0.80 \cdot \hat{\boldsymbol{\kappa}}_{\omega 33}$
$\boldsymbol{\zeta}_v = [1,\ 1 - \sin(t) - 0.5 \cdot \sin(5\,t) + 0.2 \cdot \sin(10\,t),\ 0]'$		
$\boldsymbol{\zeta}_\omega = [0,\ 1 + 0.1 \cdot \sin(t) + 0.05 \cdot \sin(5\,t) - 0.02 \cdot \sin(10\,t),\ 0]'$		
L1 adaptive control design parameters		
$L_{\rho r} = 4.8$	$\rho_r = 16.4$	$b = 13.6$
$\rho_{\text{in}} = 0.45$	$\rho_{\text{ur}} = 41.5$	$\rho = 16.6$
$\rho_u = 42.4$	$\bar{\gamma}_0 = 0.01$	$\beta = 10^{-4}$
$\bar{\gamma}_1 = 0.172$	$\gamma_1 = 0.076$	
$T_s = 10^{-5}$	$\gamma_0(T_s) = 0.0084$	$\gamma_2 = 0.60$

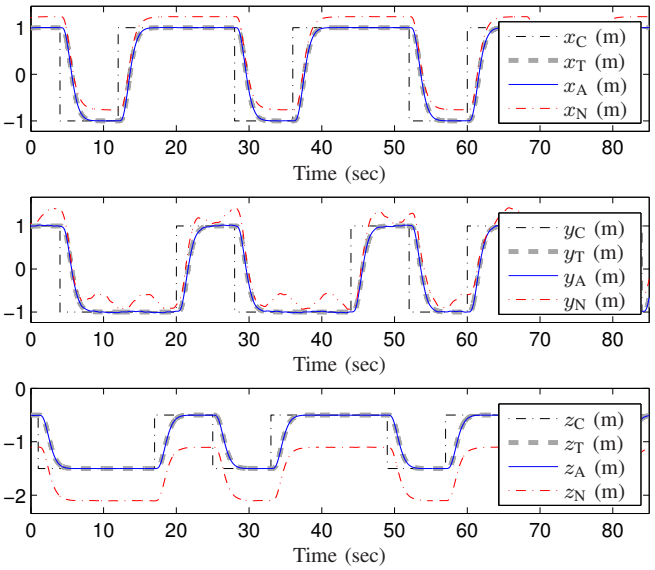

Fig. 3. Transition between the set points $\mathbf{x}_\text{C} = [x_\text{C}\ y_\text{C}\ z_\text{C}]'$ along the desired trajectory $\mathbf{x}_\text{T} = [x_\text{T}\ y_\text{T}\ z_\text{T}]'$ for the presented L1 adaptive controller $\mathbf{x}_\text{A} = [x_\text{A}\ y_\text{A}\ z_\text{A}]'$ and a nonadaptive controller $\mathbf{x}_\text{N} = [x_\text{N}\ y_\text{N}\ z_\text{N}]'$. The plant was affected by the uncertainties given in Tab. I.

Appendix

A. Proof of Lemma 1 [16, Ch. 3.2]

Proof: The transformation of (52) into the frequency domain yields $\mathbf{z}_\text{ref}(s) = \mathbf{H}(s)\mathbf{B}_f\mathbf{f}_\text{ref}(s) + \mathbf{H}(s)\mathbf{B}(\mathbf{I} - \mathbf{C}(s))\boldsymbol{\sigma}_\text{ref}(s) + \mathbf{z}_\text{in}(s) = \mathbf{H}(s)\mathbf{B}_f\mathbf{f}_\text{ref}(s) + \mathbf{G}(s)\boldsymbol{\sigma}_\text{ref}(s) + \mathbf{z}_\text{in}(s)$. The term $\mathbf{z}_\text{in}(s)$ is the Laplace transform of $\mathbf{z}_\text{in}$. An upper bound for $\mathbf{z}_\text{ref}$ for all $t \in [0, \tau]$ reads $\|\mathbf{z}_\text{ref}\|_{\mathcal{L}_\infty^{[0,\tau]}} \leq \|\mathbf{H}(s)\mathbf{B}_f\|_{\mathcal{L}_1}\|\mathbf{f}_\text{ref}\|_{\mathcal{L}_\infty^{[0,\tau]}} + \|\mathbf{G}(s)\|_{\mathcal{L}_1}\|\boldsymbol{\sigma}_\text{ref}\|_{\mathcal{L}_\infty^{[0,\tau]}} + \rho_\text{in}$ where $\tau < \infty$ is used to realize the truncated $\mathcal{L}_\infty^{[0,\tau]}$-Norm [16,

Ch. A.3]. If the bound (54) is not true, since $\|\mathbf{z}_{\text{ref}}(0)\|_\infty = \|\mathbf{z}_0\|_\infty < \rho_0 < \rho_r$ and $\mathbf{z}_{\text{ref}}$ is continuous, there exists a time $\tau_1 \in (0,\tau]$ such that $\|\mathbf{z}_{\text{ref}}(t)\|_\infty < \rho_r, \forall t \in [0,\tau_1)$ and $\|\mathbf{z}_{\text{ref}}(\tau_1)\|_\infty = \rho_r$, which implies that $\|\mathbf{z}_{\text{ref}}\|_{\mathcal{L}_\infty^{[0,\tau_1]}} = \rho_r$. For this case, we derive the upper bound

$$\max\{\|\mathbf{f}_{\text{ref}}\|_{\mathcal{L}_\infty^{[0,\tau_1]}}, \|\boldsymbol{\sigma}_{\text{ref}}\|_{\mathcal{L}_\infty^{[0,\tau_1]}}\} \leq L_{\rho r}\rho_r + b\,. \tag{74}$$

This bound leads to $\|\mathbf{z}_{\text{ref}}\|_{\mathcal{L}_\infty^{[0,\tau_1]}} \leq \|\mathbf{G}(s)\|_{\mathcal{L}_1}(L_{\rho r}\rho_r + b) + \|\mathbf{H}(s)\mathbf{B}_f\|_{\mathcal{L}_1}(L_{\rho r}\rho_r + b) + \rho_{\text{in}}$. Thus, if $\mathbf{G}(s)$ and $\mathbf{H}(s)$ satisfies (53), we have $\|\mathbf{z}_{\text{ref}}\|_{\mathcal{L}_\infty^{[0,\tau_1]}} < \rho_r$, which contradicts the assumption $\|\mathbf{z}_{\text{ref}}(\tau_1)\|_\infty = \rho_r$ and proves (54). This further implies that the upper bound (74) holds for all $t \in [0,\tau]$ with strict inequality, which in turn implies that $\|\boldsymbol{\sigma}_{\text{ref}}\|_{\mathcal{L}_\infty^{[0,\tau_1]}} < L_{\rho r}\rho_r + b$. The bound on $\mathbf{u}_{\text{ref}}$ follows from (16) and (35) and the bound above, which is $\|\mathbf{u}_{\text{ref}}\|_{\mathcal{L}_\infty^{[0,\tau]}} < \|\boldsymbol{\kappa}^{-1}\mathbf{C}(s)\|_{\mathcal{L}_1}(L_{\rho r}\rho_r + b)$ and proves (55). ■

B. Proof of Theorem 1 [16, Ch. 3.3]

Proof: Assume the bounds (72) and (73) are not true. Then, since $\|\mathbf{z}_{\text{ref}}(0) - \mathbf{z}(0)\|_\infty = 0 < \gamma_1$ and $\|\mathbf{u}_{\text{ref}}(0) - \mathbf{u}(0)\|_\infty = 0 < \gamma_2$ and $\mathbf{z}(t)$, $\mathbf{z}_{\text{ref}}(t)$, $\mathbf{u}(t)$ and $\mathbf{u}_{\text{ref}}(t)$ are continuous, there exist τ such that $\|\mathbf{z}_{\text{ref}}(\tau) - \mathbf{z}(\tau)\|_\infty = \gamma_1$ or $\|\mathbf{u}_{\text{ref}}(\tau) - \mathbf{u}(\tau)\|_\infty = \gamma_2$, while $\forall t \in [0,\tau)$ $\|\mathbf{z}_{\text{ref}}(t) - \mathbf{z}(t)\|_\infty < \gamma_1$ and $\|\mathbf{u}_{\text{ref}}(t) - \mathbf{u}(t)\|_\infty < \gamma_2$. That implies that at least one of the following equalities holds:

$$\|\mathbf{z}_{\text{ref}} - \mathbf{z}\|_{\mathcal{L}_\infty^{[0,\tau]}} = \gamma_1\,, \quad \|\mathbf{u}_{\text{ref}} - \mathbf{u}\|_{\mathcal{L}_\infty^{[0,\tau]}} = \gamma_2\,. \tag{75}$$

Then Lemma 1 implies that

$$\|\mathbf{z}_{\text{ref}}\|_{\mathcal{L}_\infty^{[0,\tau]}} \leq \rho_r\,, \quad \|\mathbf{u}_{\text{ref}}\|_{\mathcal{L}_\infty^{[0,\tau]}} \leq \rho_{ur}\,. \tag{76}$$

Using the definition of ρ and ρ_u in (69) and (70), it follows from the bounds in (75) and (76) that

$$\|\mathbf{z}\|_{\mathcal{L}_\infty^{[0,\tau]}} \leq \rho_r + \gamma_1 \leq \rho\,,\ \|\mathbf{u}\|_{\mathcal{L}_\infty^{[0,\tau]}} \leq \rho_{ur} + \gamma_2 = \rho_u\,. \tag{77}$$

Hence, if one chooses the adaptation sampling time T_s according to (66), Lemma 3.3.3 in [16] implies that

$$\|\tilde{\mathbf{z}}\|_{\mathcal{L}_\infty^{[0,\tau]}} < \bar{\gamma}_0\,. \tag{78}$$

Next, the subtraction of the Laplace transforms of (43) and (52) yields $\mathbf{z}_{\text{ref}}(s) - \mathbf{z}(s) = \mathbf{H}(s)\mathbf{B}_f(\mathbf{f}_{\text{ref}}(s) - \mathbf{f}(s)) + \mathbf{G}(s)(\boldsymbol{\sigma}_{\text{ref}}(s) - \boldsymbol{\sigma}(s)) - \mathbf{H}(s)\mathbf{B}\mathbf{C}(s)(\tilde{\boldsymbol{\sigma}}(s) + \tilde{\boldsymbol{\kappa}}\mathbf{u}(s))$. Furthermore, if follows from the error dynamics in (60) that

$$\tilde{\boldsymbol{\sigma}}(s) + \tilde{\boldsymbol{\kappa}}\mathbf{u}(s) = (s\mathbf{I} - \mathbf{A}_e)\tilde{\mathbf{z}}(s) =: \mathbf{H}_e^{-1}(s)\tilde{\mathbf{z}}(s) \tag{79}$$

Therefore, we have

$$\|\mathbf{z}_{\text{ref}} - \mathbf{z}\|_{\mathcal{L}_\infty^{[0,\tau]}} \leq \|\mathbf{H}(s)\mathbf{B}_f\|_{\mathcal{L}_1}\|\mathbf{f}_{\text{ref}} - \mathbf{f}\|_{\mathcal{L}_\infty^{[0,\tau]}} + \|\mathbf{G}(s)\|_{\mathcal{L}_1} \cdot \|\boldsymbol{\sigma}_{\text{ref}} - \boldsymbol{\sigma}\|_{\mathcal{L}_\infty^{[0,\tau]}} + \|\mathbf{H}(s)\mathbf{B}\mathbf{C}(s)\mathbf{H}_e^{-1}(s)\|_{\mathcal{L}_1}\|\tilde{\mathbf{z}}\|_{\mathcal{L}_\infty^{[0,\tau]}}. \tag{80}$$

With $\bar{\rho}_r(\rho_r)$ defined as in (47), it follows, $\|\mathbf{z}\|_{\mathcal{L}_\infty^{[0,\tau]}} \leq \rho_r + \gamma_1 \leq \rho_r + \bar{\gamma}_1 = \bar{\rho}_r(\rho_r)$ and $\|\mathbf{z}_{\text{ref}}\|_{\mathcal{L}_\infty^{[0,\tau]}} \leq \rho_r < \bar{\rho}_r(\rho_r)$. The definitions of (45) and (46) imply that the following upper bound exists

$$\max\{\|\mathbf{f}_{\text{ref}} - \mathbf{f}\|_{\mathcal{L}_\infty^{[0,\tau]}}, \|\boldsymbol{\sigma}_{\text{ref}} - \boldsymbol{\sigma}\|_{\mathcal{L}_\infty^{[0,\tau]}}\} < L_{\rho_r}\|\mathbf{z}_{\text{ref}} - \mathbf{z}\|_{\mathcal{L}_\infty^{[0,\tau]}}\,. \tag{81}$$

With this bound and (78), (80) leads to the upper bound

$$\|\mathbf{z}_{\text{ref}} - \mathbf{z}\|_{\mathcal{L}_\infty^{[0,\tau]}} \leq \frac{\|\mathbf{H}(s)\mathbf{B}\mathbf{C}(s)\mathbf{H}_e^{-1}(s)\|_{\mathcal{L}_1}}{1 - (\|\mathbf{G}(s)\|_{\mathcal{L}_1} + \|\mathbf{H}(s)\mathbf{B}_f\|_{\mathcal{L}_1})L_{\rho_r}}\,\bar{\gamma}_0\,.$$

Note that $(\|\mathbf{G}(s)\|_{\mathcal{L}_1} + \|\mathbf{H}(s)\mathbf{B}_f\|_{\mathcal{L}_1})L_{\rho_r} < 1$ holds due to condition (53). Along with the definition of γ_1 from (65) we obtain

$$\|\mathbf{z}_{\text{ref}} - \mathbf{z}\|_{\mathcal{L}_\infty^{[0,\tau]}} \leq \gamma_1 - \beta < \gamma_1\,. \tag{82}$$

For the upper bound in (70), it follows from (16) and (35) that $\mathbf{u}_{\text{ref}}(s) - \mathbf{u}(s) = -\boldsymbol{\kappa}^{-1}\mathbf{C}(s)(\boldsymbol{\sigma}_{\text{ref}}(s) - \boldsymbol{\sigma}(s)) + \boldsymbol{\kappa}^{-1}\mathbf{C}(s)(\tilde{\boldsymbol{\sigma}}(s) + \tilde{\boldsymbol{\kappa}}\mathbf{u}(s))$. One can write, using (79), $\|\mathbf{u}_{\text{ref}}(s) - \mathbf{u}(s)\|_{\mathcal{L}_\infty^{[0,\tau]}} = \|\boldsymbol{\kappa}^{-1}\mathbf{C}(s)\|_{\mathcal{L}_1}\|\boldsymbol{\sigma}_{\text{ref}} - \boldsymbol{\sigma}\|_{\mathcal{L}_\infty^{[0,\tau]}} + \|\boldsymbol{\kappa}^{-1}\mathbf{C}(s)\mathbf{H}_e^{-1}(s)\|_{\mathcal{L}_1}\|\tilde{\mathbf{z}}\|_{\mathcal{L}_\infty^{[0,\tau]}}$. With (81), (82) and (78)

$$\|\mathbf{u}_{\text{ref}}(s) - \mathbf{u}(s)\|_{\mathcal{L}_\infty^{[0,\tau]}} = \|\boldsymbol{\kappa}^{-1}\mathbf{C}(s)\|_{\mathcal{L}_1}L_{\rho_r}(\gamma_1 - \beta) + \|\boldsymbol{\kappa}^{-1}\mathbf{C}(s)\mathbf{H}_e^{-1}(s)\|_{\mathcal{L}_1}\bar{\gamma}_0 < \gamma_2\,. \tag{83}$$

Finally, we note that the upper bounds in (82) and (83) contradict the equalities in (75) and thus prove the bounds in (69) and (70). The results in (71) - (73) follow directly from the bounds in (77). ■

REFERENCES

[1] J. Hauser, S. Sastry, and G. Meyer, "Nonlinear control design for slightly non-minimum phase systems: Application to v/stol aircraft," *Automatica*, vol. 28, pp. 665 – 679, 1992.

[2] D. Lee, H. J. Kim, and S. Sastry, "Feedback linearization vs. adaptive sliding mode control for a quadrotor helicopter," *International Journal of Control, Automation, and Systems*, vol. 7, pp. 419–428, 2009.

[3] I. Fantoni and R. Lozano, *Non-linear Control for Underactuated Mechanical Systems*, E. Sontag and M. Thoma, Eds. Springer, 2002.

[4] M. Krstic, I. Kanellakopoulos, and P. Kokotovic, *Nonlinear and Adaptive Control Design*. John Wiley & Sons, Inc., 1995.

[5] E. Frazzoli, M. Dahleh, and E. Feron, "Trajectory tracking control design for autonomous helicopters using a backstepping algorithm," in *Proceedings of the American Control Conference*, 2000.

[6] T. Hamel, R. Mahony, R. Lozano, and J. Ostrowski, "Dynamic modelling and configuration stabilization for an X4-Flyer," in *Proceedings of the 15th IFAC World Congress*, 2002.

[7] R. Mahony and T. Hamel, "Adaptive compensation of aerodynamic effects during takeoff and landing manoeuvres for a scale model autonomous helicopter," *European Journal of Control*, vol. 7, pp. 1 – 15, 2001.

[8] T. Madani and A. Benallegue, "Adaptive control via backstepping technique and neural networks of a quadrotor helicopter," in *Proceedings of the 17th IFAC World Congress*, 2008.

[9] J. Pflimlin, T. Hamel, P. Soueres, and R. Mahony, "A hierarchical control strategy for the autonomous navigation of a ducted fan flying robot," in *Proceedings of the IEEE International Conference on Robotics and Automation*, 2006.

[10] A. Roberts and A. Tayebi, "Adaptive position tracking of vtol uavs," *IEEE Transactions on Robotics*, vol. 27, pp. 129 – 142, 2011.

[11] D. Lee, C. Nataraj, T. Burg, and D. Dawson, "Adaptive tracking control of an underactuated aerial vehicle," in *Proceeding of the American Control Conference*, 2011.

[12] K. Aström and B. Wittenmark, *Adaptive control*. Dover Publications, Inc., 2008.

[13] I. N. M. Papadakis and S. C. A. Thomopoulos, "Modified output error method with parameter mismatch compensation for improved performance model reference adaptive control," in *Proceedings of the 31st IEEE Conference on Decision and Control*, 1992.

[14] J. Sun, "A modified model reference adaptive control scheme for improved transient performance," *IEEE Transactions on Automatic Control*, vol. 38, no. 8, pp. 1255 –1259, aug 1993.

[15] B. Ydstie, "Transient performance and robustness of direct adaptive control," *IEEE Transactions on Automatic Control*, vol. 37, pp. 1091–1105, 1992.

[16] N. Hovakimyan and C. Cao, *L1 Adaptive Control Theory: Guaranteed Robustness With Fast Adaptation*, R. C. Smith, Ed. SIAM - Society for Industrial and Applied Mathematics, 2010.

[17] N. Hovakimyan, C. Cao, E. Kharisov, E. Xargay, and I. Gregory, "L1 adaptive control for safety-critical systems," *IEEE Control Systems Magazine*, vol. 31, pp. 54 –104, 2011.

[18] X. Wang and N. Hovakimyan, "L1 adaptive controller for nonlinear time-varying reference systems," *Systems & Control Letters*, vol. 61, pp. 455 – 463, 2012.